analytical chemistry

Article

Cite This: Anal. Chem. 2017, 89, 11653-11663

pubs.acs.org/ac

Elasto-Inertial Focusing of Mammalian Cells and Bacteria Using Low Molecular, Low Viscosity PEO Solutions

Gregor Holzner, Stavros Stavrakis,* and Andrew deMello*

Institute for Chemical and Bioengineering, Department of Chemistry and Applied Biosciences, ETH Zürich, Vladimir Prelog Weg 1, 8093 Zürich, Switzerland

Supporting Information

ABSTRACT: The ability to manipulate biological cells is critical in a diversity of biomedical and industrial applications. Microfluidic-based cell manipulations provide unique opportunities for sophisticated and high-throughput biological assays such as cell sorting, rare cell detection, and imaging flow cytometry. In this respect, cell focusing is an extremely useful functional operation preceding downstream biological analysis, since it allows the accurate lateral and axial positioning of cells moving through microfluidic channels, and thus enables sophisticated cell manipulations in a passive manner. Herein, we explore the utility of viscoelastic carrier fluids for enhanced elasto-inertial focusing of biological species within straight, rectangular cross section microfluidic channels. Since the investigated polymer solutions possess viscosities close to that of water and exhibit negligible shear thinning, focusing occurs over a wide range of elasticity numbers and a large range of Reynolds numbers. With a view to applications in the robust focusing of cells and bacteria, we assess and characterize the influence of accessible focusing parameters, including blockage ratio, volumetric flow rate, cell concentration, and polymer chain length.

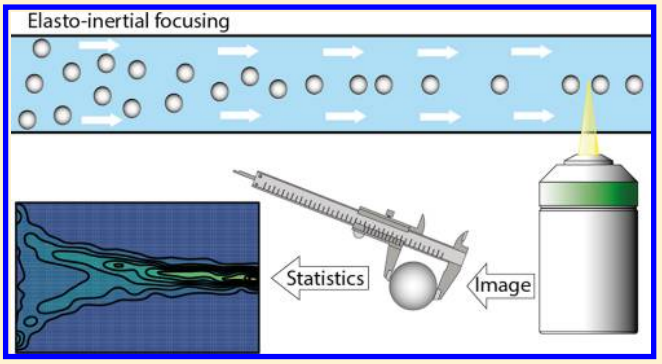

Over the past decade, microfluidic systems have proven to be powerful tools in the high-throughput and high-efficiency analysis of single cells and macromolecules, with applications in sorting/isolation,[1−5] optical characterization,[6,7] and mechanical phenotyping[8−10] of large and heterogeneous populations. Recently, hydrodynamic effects, most notably fluid inertia[11] and elasticity,[12] have been utilized to good effect in microfluidic devices to focus and separate cells by driving them laterally toward stable equilibrium positions.

Particle migration in Newtonian media was first observed over five decades ago by Segre[13] but has only recently been exploited within microscale flows. Microfluidic technologies that rely on fluid inertia have resulted in interesting new effects, such as the formation of multiple "equilibrium" positions or the ordering of cells in the direction of flow. Critically, inertial focusing of cells affords high-throughput processing, while maintaining cell viability and minimizing cell damage.[14] For certain applications, such as flow cytometry, that require cells to be confined within the focal plane of an optical detection system, curved channels or multiheight structures have been successfully used to induce secondary flows and promote single-cell focusing in rectangular channels.[15,16]

That said, the increased complexity of these systems in combination with the high flow rates needed for efficient focusing complicate their facile implementation in imaging flow cytometers. For these reasons, cell manipulations in viscoelastic fluids have gained increasing attention, due to the fact that three-dimensional focusing in straight microchannels can be realized in a simple fashion. For example, Karnis and Mason[17] found that rigid particles will migrate in the direction of decreasing shear rate in both Couette and Poiseuille flows when using fully viscoelastic fluids. The authors suggested that this behavior is a result of normal stress differences, since migration did not occur in Newtonian fluids. The role of normal stress differences on particle migration in Poiseuille flows was later elucidated by Ho and Leal[18] and Morris and Boulay.[19] Specifically, migration of particles in nonhomogeneous shear flows occurs because of a spatially varying shear rate, involving variations in the first normal stress difference, N1. Such variations in N1 result in a force in the direction of decreasing shear rate, which is directed toward the center of a circular channel[20,21] or toward the centerline in a slit geometry channel.[12] Based on these studies, viscoelastic focusing is expected to be a valuable tool in controllable 3D particle focusing.

Recent studies have shown that fluid inertia and fluid elasticity can interact to stabilize a flow if present simultaneously. For example, Yang et al.[22] demonstrated elasto-inertial particle focusing in planar rectangular channels using dilute polymer solutions. Migration from multiple equilibrium positions to a single particle stream along the channel

Received: August 2, 2017
Accepted: October 5, 2017
Published: October 5, 2017

DOI: 10.1021/acs.analchem.7b03093
Anal. Chem. 2017, 89, 11653−11663

centerline was observed when elastic and inertial forces were synergistically balanced.[22] More recently, Kim and Kim[23] used a λ-DNA solution as a viscoelastic carrier fluid and showed that elasto-inertial particle focusing (at Reynolds numbers between 1 and 5 and elasticity numbers between 10 and 100) is destabilized as Reynolds numbers increase. To test whether such elasto-inertial effects can enable particle migration in microfluidic flows at high Reynolds numbers, Lim et al.[24] used hyaluronic acid as a viscoelastic, drag-reducing additive and experimentally assessed particle behavior at flow speeds up to 130 m/s. They showed that when both elasticity and inertia are present, particle focusing can be accomplished at flow rates much higher than previously achieved. Another recent study by Seo et al.[25] showed that the flow rate, blockage ratio, and shear-thinning properties of viscoelastic fluids have complex effects on particle migration within square cross section channels in the presence of both elastic and inertial forces. However, parameters such as fluid elasticity, shear-dependent viscosity, and the interplay between blockage ratio and cell concentration, which all affect the efficiency of single-line cell focusing have yet to be thoroughly investigated.

Controlled particle manipulation in microfluidic channels using viscoelastic fluids can be achieved by controlling the channel geometry, particle geometry, and fluid rheology. Lim et al.[24] elucidated operating parameters for elasto-inertial focusing that report the dependency of particle migration on both the Reynolds number (Re) and Weissenberg number (Wi). The authors suggested that an Elastic Number (El) > 1 describes an elastically dominated flow, whereas an El < 1 describes an inertially dominated flow. Moreover, results were compared with previous studies of particle migration in viscoelastic fluids (in both the presence and absence of inertia), in which particle focusing deteriorates when Re > 1.[21,22] Based on this comparison, it is evident that an unexplored regime exists (Re > 1, 0.1 < Wi < 3 and 0.1 < El < 2) where the mechanism of cell migration needs further investigation. Furthermore, the effective limits of elasto-inertial focusing are still poorly defined in terms of Wi−Re state space. Inertial focusing typically occurs in Newtonian fluids, with an upper limit at $Re \approx 1500$[26] (meaning that Wi = 0 and El < 1). Viscoelastic focusing typically occurs for Re < 1 but has also been observed in the presence of non-negligible inertia,[21,22] with $El \gg 1$ in either case. Assessment of the unexplored regime (Re > 1, 0.1 < Wi < 3, and 0.1 < El < 2) will allow for the characterization of viscoelastic focusing in the (extremely) low elasticity regime, where the effect of shear thinning becomes negligible.

One of the primary drivers for research on cell migration within microfluidic devices is the potential for application in high-throughput flow cytometry. Despite the robustness of particle focusing in non-Newtonian fluids, its practical implementation in real-world applications such as imaging flow cytometry has yet to be fully explored. Accordingly, herein we assess viscoelastic particle focusing using an aged,[27] low molecular weight poly(ethylene oxide) (PEO) in a previously unexplored flow regime, with weakly elastic fluids ($El \approx 0.3$) and non-negligible inertia (Re = 0.4−10) and elasticity (Wi = 0.1−3.1). Significantly, the shear viscosity of a 500 ppm PEO (0.4 MDa) polymer solution is invariant over a wide range of shear rates, meaning that stable focusing is achievable at high flow rates despite the low viscosity. In addition to studying the migration dynamics of cells in viscoelastic media (using different molecular weight PEOs), we also explore the influence of blockage ratio and cell concentration on migration behavior from the moment that the cell stream enters the channel. To demonstrate the utility of viscoelastic PEO solutions, we assess single bacteria focusing using stroboscopic epifluorescence imaging.

MOTIVATION

The ultimate goal of the current study is to use the presented cell focusing method in imaging flow cytometry. The performance of imaging flow cytometers[28,29] or image based cell-sorters[30,31] can be quantified using a range of parameters such as analytical throughput, imaging resolution, detection modality (e.g., bright-field, dark-field, and fluorescence), and system complexity. Not surprisingly, analytical throughput should ideally be as high as possible but will be limited by camera frame rates/exposure times and by the capabilities of the focusing system. Commercial flow cytometers almost always implement hydrodynamic focusing to position cells within the fluidic path. Although such an approach has been shown to allow for both two- and three-dimensional focusing and high-throughput cellular analysis, the ability to supply large volumes of sheath fluid, while maintaining a defined pressure drop, remains a significant drawback. In the current work, we aim to demonstrate that cells migrate from streamlines and focus at the center of a microfluidic channel using passive elasto-inertial forces and a single input stream. We show that throughput limitations using elasto-inertial focusing schemes are defined not only by geometrical constraints and the rheological properties of the carrier fluid but also on other factors, most notably the formation of cell packages. Imaging resolution is defined by the optics, the pixel size of the sensor, and the flow velocity, noting that the position distribution of the cell stream must be smaller than the depth of field of the objective for efficient analysis. In general, we aim to achieve single-file focusing of cells (or other micron-sized objects), over a wide range of flow velocities and in a simple manner.

DIMENSIONLESS NUMBERS

The characterization of fluids in motion can be most easily assessed by consideration of dimensionless numbers. To describe the flow of viscoelastic fluids three numbers are especially important: the channel Reynolds number (Re), the Weissenberg number (Wi) and the Elasticity number (El). The channel Reynolds number for a pipe can be defined according to

$$Re = \frac{\rho v D_h}{\eta} \tag{1}$$

where v is the fluid velocity, D_h the hydraulic diameter ($= 2wh/(h + w)$) where h and w represent the channel height and width, respectively, ρ is the fluid density, and η is the dynamic viscosity, with Re quantifying the relative importance of inertial forces with respect to viscous forces. Similarly, the Weissenberg number assesses the relative importance of elastic and viscous forces and is defined as

$$Wi = \lambda\dot{\gamma} = \frac{2\lambda Q}{hw^2} = \lambda\frac{2V}{w} \tag{2}$$

where λ is the relaxation time of the fluid, $\dot{\gamma}$ is the characteristic shear rate ($\dot{\gamma} = 2Q/hw^2$), and Q is the volumetric flow rate. In simple terms, the higher the Weissenberg number, the more elastic the fluid is.

DOI: 10.1021/acs.analchem.7b03093
Anal. Chem. 2017, 89, 11653−11663

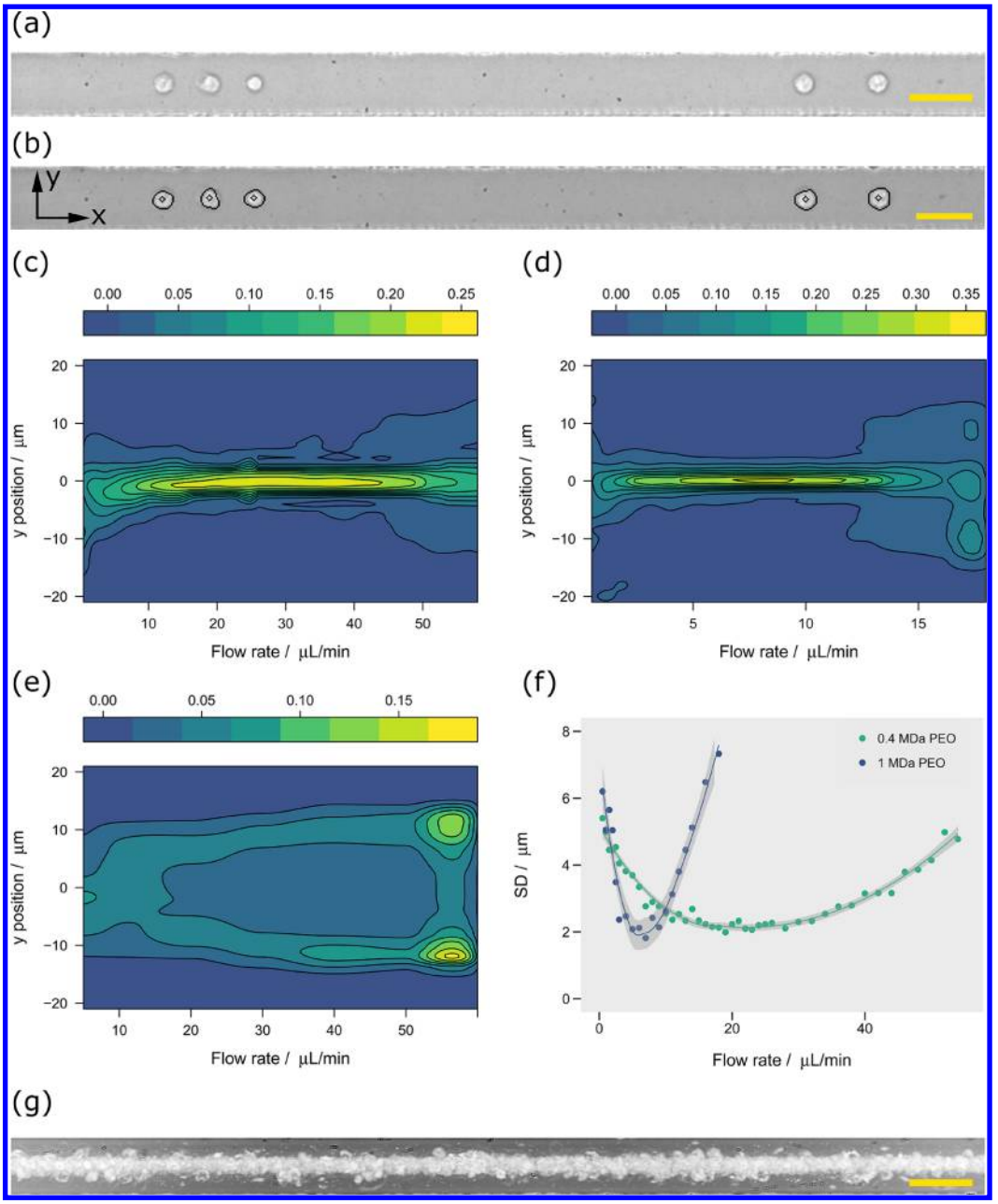

Figure 1. (a) Raw images of cells moving at a velocity of ~0.1 m/s. (b) Processed images highlighting cell contours and centroids. Panels (c–e) show the distribution of HL60 cells along perpendicular to flow direction at different flow rates. The colormap indicates the density of the distribution. (c) PEO carrier solution (500 ppm, 0.4 MDa) with a cell concentration of 1 000 000 per mL (Re = 0.4–10.3, Wi = 0.1–3.12, El = 0.3). (d) PEO carrier solution (500 ppm, 1 MDa) with a cell concentration of 1 000 000 per mL (Re = 0.08–2.98, Wi = 0.17–6.36, El = 2.1–2.2). (e) Solution without PEO (Newtonian solution, Re = 0.4–10.3, Wi = 0) shows for higher flow rates (>20 μL/min) two files of cells close to the walls of the square channel (four files, one on the center of each channel wall, appear as two files because the others are not in the focal plane). (f) Standard deviation (SD) in y direction of the heat maps shown in (c) and (d) as green (0.4 MDa PEO) and blue (1 MDa PEO), respectively. (g) Image stack of cells flowing at 30 μL/min in a 500 ppm, 0.4 MDa PEO solution. Scale bars are 50 μm.

To achieve effective focusing of particles, elastic forces and inertial forces must be balanced. Since fluid elasticity and inertia are represented by Wi and Re, the elasticity number El can be used to measure the relative importance of elastic forces to inertial effects and is given by

$$El = \frac{Wi}{Re} = \frac{\lambda\eta(w + h)}{\rho w^2 h} \tag{3}$$

Elasticity numbers close to zero describe inertia dominant regimes, whereas elasticity numbers greater than 1 describe situations where elastic forces dominate. In a flow with non-negligible inertia, particles will be focused along the channel centerline due to a combination of fluid elasticity and wall repulsion forces arising from fluid inertia.[22]

EXPERIMENTAL SECTION

Cell Culture. Experiments were performed using HL-60 and Human B-lymphoid cell lines (Sigma-Aldrich, Switzerland). All cell lines were initially tested for mycoplasma contamination and then cultured according to standard protocols. All

DOI: 10.1021/acs.analchem.7b03093
Anal. Chem. 2017, 89, 11653–11663

experiments were performed on cells in the exponential (log) phase of growth. For all experiments, cells were fixed with formaldehyde, and an OptiPrep density gradient medium (Sigma-Aldrich, Switzerland) was added to prevent sedimentation. Final solutions consisted of DPBS buffer (Life Technologies, Switzerland) containing 36% (v/v) OptiPrep, fixed cells (0.5−12 Mio/mL), and 500 ppm PEO (0.4 or 1 MDa). We prefer to use fixed cells, because they tend to be more stable and are not lysed during flow manipulation. A sample with fixed cells can also be used over several days without any deterioration. That said, we also performed experiments with living cells and observed the same focusing behavior as with fixed cells.

Bacteria Culture. *E. coli* BL21 (DE3) (BioConcept, Switzerland) were transformed with the plasmid pEXP5-NT/mCherry, a gift from Dr. Dora Tang (MPI-CBG, Dresden, Germany), following a standard protocol. Bacteria were grown in Lysogeny Broth (LB) overnight at 37 °C while vigorously shaking. For experiment, bacteria were fixed with formaldehyde and immersed into DPBS (Dulbecco's Phosphate-Buffered Saline) solution.

Viscoelastic Solutions. Viscoelastic master solutions were prepared by thoroughly dissolving low molecular weight poly(ethylene oxide) (M_w = 0.4 × 10^6 g/mol and 1 × 10^6 g/mol—Sigma-Aldrich, Switzerland) in phosphate-buffered DPBS solutions (Life Technologies, Switzerland) to a concentration of 10 g/L. Solutions were allowed to age at room temperature for one month to achieve uniform viscosities.[27] Master solutions (10 g/L) were diluted before experiment to a concentration of 500 ppm. Viscosities were measured with a modular compact rheometer (Anton Paar MCR 502, Germany) using a double gap (DG 26.7) tool. The viscosity of the pure DPBS/OptiPrep solution was 1.57 mPa·s, the viscosity of 0.4 MDa PEO/DPBS/OptiPrep was 1.9 mPa·s, and the viscosity of 1 MDa PEO/DPBS/OptiPrep was between 2.2 and 2.1 mPa·s, depending on the shear rate (Figure S-1). Relaxation times of dilute solutions were below the detection limit of the rheometer and were thus estimated as described in the Supplemental Note S-1.

Device Fabrication. Microfluidic devices were fabricated using standard soft-lithographic techniques. A 10:1 mixture of polydimethoxysilane (PDMS) monomer and curing agent (Sylgard 184, Dow Corning, Midland, MI, U.S.A.) was poured over a master-mold and peeled off after polymerization at 70 °C for 4 h. Inlet and outlet ports were punched using a hole-puncher, and the PDMS substrate was bonded to a planar glass substrate (Menzel-Glaser, Germany) after treating both surfaces with an oxygen plasma (EMITECH K1000X, Quorum Technologies, U.K.) for 60 s.

Device Operation and Data Acquisition. The cell/bacteria suspension was loaded into a 1 mL syringe (Gastight Syringes, Hamilton Laboratory Products, Reno, NV, U.S.A.) and delivered at the desired flow rate using a precision syringe pump (Harvard Apparatus, Holliston, MA, U.S.A.). The microfluidic device was mounted on an inverted microscope (Eclipse Ti-E, Nikon, Zürich, Switzerland) equipped with a high speed camera (IDT Motion Pro Y5.1, Niederoenz, Switzerland) and a CMOS camera (ORCA-flash 4.0, Hamamatsu, Solothurn, Switzerland). Bright-field imaging of cells was carried out using the IDT high-speed camera, illumination from a plasma light source (Thor Laboratories, HPLS200 Series) and a 20×, 0.45 NA objective (S Plan Fluor, Nikon, Zürich, Switzerland).

Fluorescence imaging was achieved using the CMOS camera in combination with a stroboscopic illumination source, comprising a 100 mW 532 nm LASER (Coherent Sapphire), an acoustooptical tunable filter (AOTFnC-400−650-TN, AA Optoelectronic, Orsay, France) and a 60×, 1.20 NA WI objective (Plan Apo, Nikon, Zürich, Switzerland). For a higher magnification, the 1.5× magnification mode of the microscope was used, yielding a total magnification of 90×. Resulting images of cells and bacteria were analyzed using in house Python scripts and the computer vision library OpenCV (opencv.org).

RESULTS AND DISCUSSION

Effect of Polymer Length. To confirm 3-D particle focusing in microfluidic channels, the lateral distribution of HL60 cells (Figure 1a,b) was examined at different average flow rates (Q). We first evaluated the effect of polymer length on focusing efficiency using 500 ppm solutions of 0.4 and 1 MDa PEO, a blockage ratio of 0.24, and flow rates ranging from 0.2 to 55 μl/min (Re = 0−8, Wi = 0.17−30). The corresponding elasticity numbers were calculated to be 0.3 and 2.1−2.2 for the 0.4 and 1 MDa PEO samples, respectively. Statistical particle distributions (across the channel in the y-direction) of an HL60 cell population at various flow rates and molecular weights are illustrated in Figure 1c,d. Similar behavior is observed for both PEO samples, namely, at low volumetric flow rates, cells are initially distributed across the majority of the channel cross section. As the flow rate is increased, this distribution narrows, reaching a minimum and then broadening with any further increase in volumetric flow rate. However, the viscosity of the two PEO solutions has a different dependency on shear rate. Specifically, the shear viscosity of the 0.4 MDa PEO solution is approximately constant over a wide range of shear rates, while that of the 1 MDa PEO shows some shear-thinning behavior (Figure S-1). Accordingly, cell migration in the low molecular weight PEO solution is expected to be different to that in the higher molecular weight PEO solution. This prediction agrees with previous experimental observations, which indicate that the shear-thinning effect drives particles closer to the microchannel wall when suspended in viscoelastic fluids.[32,33]

When cells are suspended in the uniform viscosity solution (500 ppm, 0.4 MDa PEO) and motivated at flow rates between 1 and 10 μL/min (Re = 0.4−1.8), cells remain well distributed over the channel cross section, weakly migrating to channel walls (Figure 1c). As the flow rate increases (from 10 to 40 μl/min, Re = 1.8−7.4, Wi = 0.54−2.26), the distribution of the cells across the channel cross section narrows to a single file close to the channel centerline (approximately 17 μm in width; Figure 1g, with cells having an average diameter of 13 μm). Figure 1e illustrates the cell migration behavior in a Newtonian fluid, showing that inertial focusing starts at approximately 20 μL/min, and demonstrating that the 0.4 MDa PEO solution focuses at flow rates up to those used for pure inertial focusing (Figure 1e).

An interesting feature of Figure 1c is that focusing at the channel centerline remains tight over a wide range of flow rates and up to 40 μL/min (Re = 7, cell velocity ≈ 0.13 m/s). At flow rates between 22 and 30 μL/min, 86.2% of the cell's center points are within ±2.5 μm of the center of the channel (Figure 1g). Focusing performance marginally deteriorates at flow rates above 33 μl/min (84.4% within ±2.5 μm), but is still more than adequate for applications in high-throughput flow cytometry. At flow rates exceeding 40 μL/min (Re > 8, Wi = 2.47−3.12),

DOI: 10.1021/acs.analchem.7b03093
Anal. Chem. 2017, 89, 11653−11663

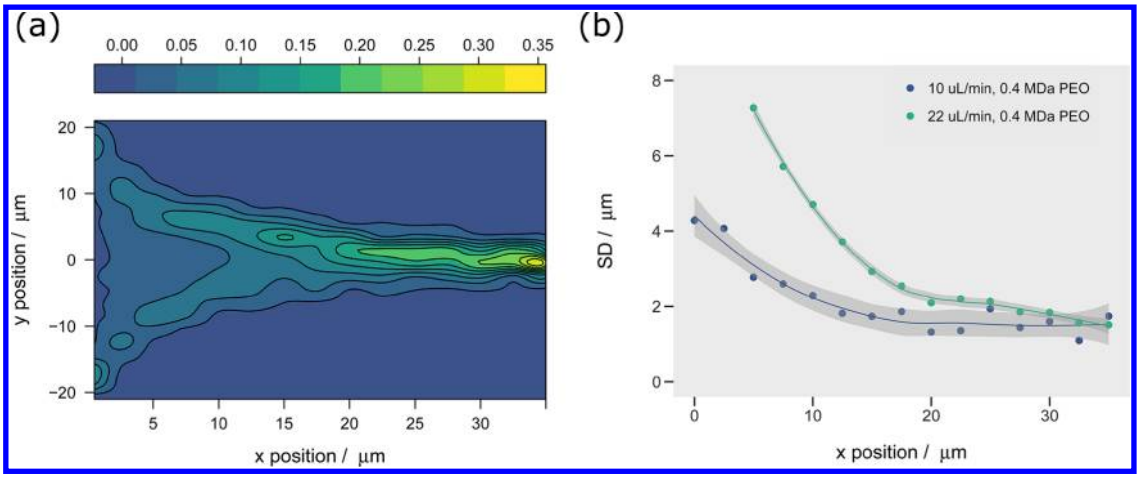

Figure 2. (a) Distribution of cells across the channel cross section (53 × 53 μm) as a function of distance from inlet for a 500 ppm, 0.4 MDa PEO carrier solution with a cell concentration of 1 000 000 cells/mL at a flow rate of 22 μL/min. The colormap indicates the density of the distribution. (b) Standard deviation of cell distribution in y direction as a function of distance from the inlet for two flow rates: 10 μL/min (Re = 1.8, Wi = 0.54, El = 0.3) and 22 μL/min (Re = 3.9, Wi = 1.18, El = 0.3).

focusing along the centerline significantly deteriorates, with cells migrating to off-center positions. To compare the behavior of particles and cells under the same flow conditions, we performed additional experiments using rigid polystyrene (PS) beads (Figure S-2). Results indicate that PS particles are efficiently focused to a single line when using a 1000 ppm PEO solution. This contrasts with the observation that cells can be focused when using a 500 ppm PEO solution (see Supplemental Note S-2 for more details).

We used a 20× 0.45 NA objective in combination with a camera having a pixel size of 7 × 7 μm, leading to a theoretical resolution of 0.35 μm per pixel and a depth of field close to 3 μm. This value is larger than the standard deviation of the position distribution of the cell stream, which means that we can efficiently focus cells within the depth of field of the objective used. The efficiency was measured by determining the distribution of cell centroid points across the channel width (denoted as y in Figure 1b). The standard deviation, SD, of this distribution (we define an SD of 2.5 μm as being "good", see Figure S-3) served as the metric to define efficiency.

For the higher molecular weight PEO solution, cells were tightly focused along the channel centerline at low flow rates ranging from 2 to 10 μL/min, with focusing efficiency deteriorating at flow rates exceeding 10 μL/min. A similar focusing behavior has previously been observed in microchannel flows with $Re \approx 0-0.1$ and $El \approx 10-100$,[12,20−22,33] in simulations,[33,34] and more recently in flows with $Re \approx 1000$ and $El \approx 10^{-1}$.[24] Previous studies have also suggested that when the suspending medium is shear thinning, particles or cells will only be tightly focused along the channel centerline at flow rates below those of pure inertial focusing in non-Newtonian fluids.[25] Accordingly, particle migration behavior in the 1 MDa PEO solution is consistent with previous observations in shear-thinning fluids, and thus, we attribute the defocusing observed at higher flow rates (>10 μL/min) to the shear-thinning behavior of the carrier fluid. This hypothesis agrees with the measured shear-thinning behavior of the 1 MDa PEO solution (Figure S-1). Under the present experimental conditions, for the shear-thinning fluid, El varies between 2.2 to 2.1 as the flow rate increases from 0.5 to 18.5 μL/min. This decrease in El is caused by a reduction in shear viscosity with increasing flow rate. A decreasing El means that inertial effects gradually become more significant as flow rate increases in a shear-thinning fluid. Accordingly, inertial effects overcome elastic forces and the particle distribution becomes wider (Figure 1d,f). At a fixed flow rate, Wi increases and Re decreases with increasing polymer length (Supplemental Table S-2), since both relaxation time and viscosity increase with molecular weight. El increases with increasing polymer length, and a cell suspended in a polymer solution of higher molecular weight (1 vs 0.4 MDa herein) will focus at the centerline more quickly than a cell suspended in a lower molecular weight polymer solution.

Figure 1f shows that the 1 MDa PEO solution (blue curve in Figure 1f) focuses slightly better at 9 μL/min (91% within ±2.5 μm) than the 0.4 MDa PEO solution (85% within ±2.5 μm) at 22 μL/min. This is most likely the result of stronger elastic forces within the 1 MDa PEO solution and the lower flow velocity. However, when manipulating viable living cells, it is beneficial to use low viscosity solutions, so as to avoid aggregation. Furthermore, it can be seen that the 0.4 MDa PEO solution offers the widest range of flow rates that allow single-line focusing reported to date.

It is important to note that Kim[23] and Kang[21] used solutions with long relaxation times (5 ppm λ-DNA, λ = 0.14 s) to obtain efficient focusing over a wide range of flow rates (10−20 μL/min for 15 μm particles[23]), since dilute DNA solutions act as viscoelastic fluids having a constant shear viscosity. In the current study, we found that an aged[27] 500 ppm, 0.4 MDa PEO solution in combination with OptiPrep exhibits an almost identical elastic behavior to λ-DNA, costs significantly less, and can operate over a much wider range of flow rates (Figure 1f).

Dynamic Focusing. We aimed to make the microfluidic channel design as simple as possible to ensure robust operation and thus kept the length of the channel as short as possible. Accordingly, it is important to know how quickly particles or cells migrate to the channel centerline after entry. As noted by D'Avino,[33] the particle distribution across the channel cross section depends on distance from the inlet. Figure 2a shows cell distributions vs flow direction for HL60 cells in a 500 ppm, 0.4 MDa PEO carrier solution at a flow rate of 22 μL/min. Initially, cells close to the inlet are distributed radially, with some bias to the channel walls. Also, the flow rate impacts the migration of cells to the centerline of the channel, as shown in Figure 2b. At

DOI: 10.1021/acs.analchem.7b03093
Anal. Chem. 2017, 89, 11653−11663

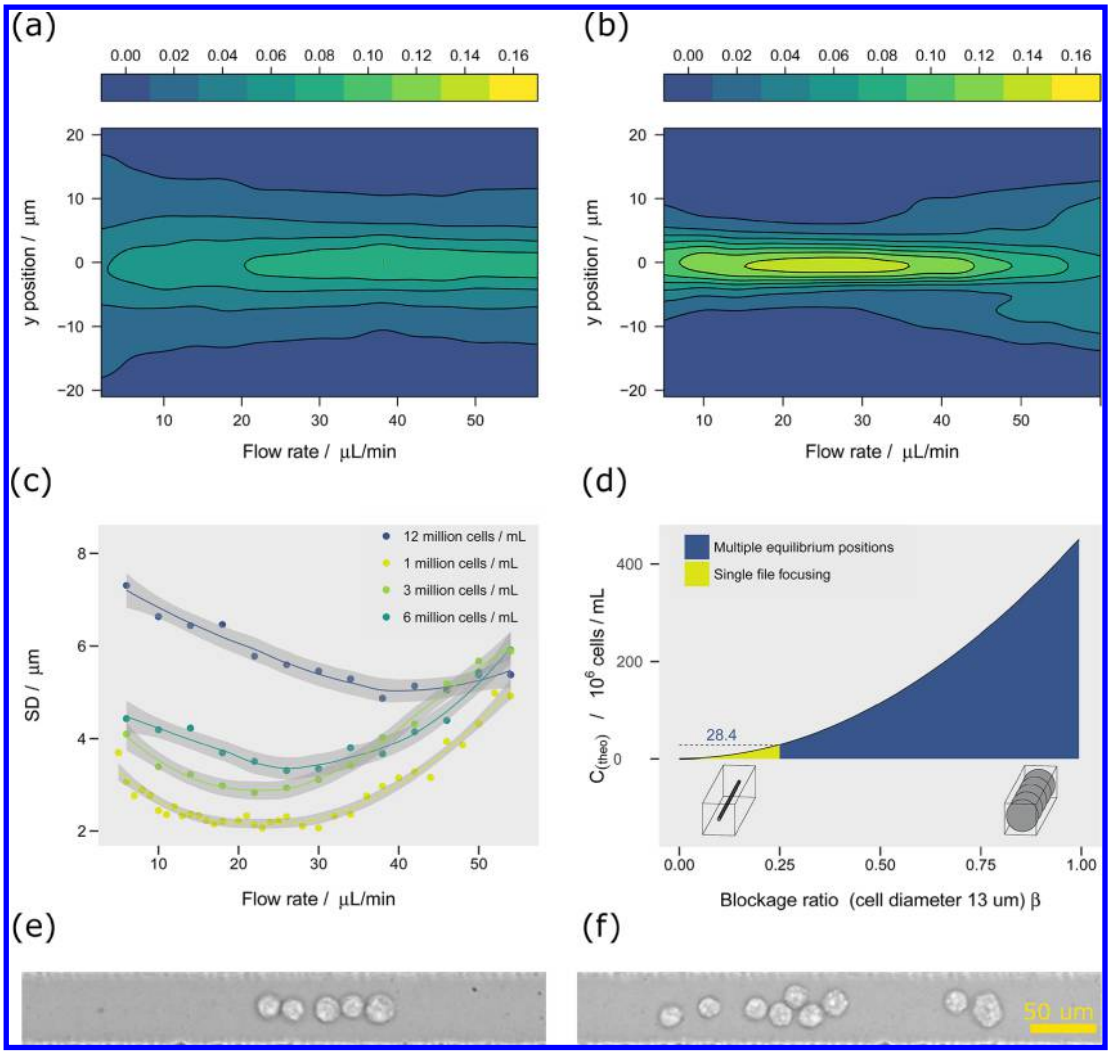

Figure 3. Distribution of HL60 in y direction with a concentration of (a) 12 000 000 cells/mL and (b) 3 000 000 cells/mL at different flow rates. The colormap indicates the density of the distribution. (c) Standard deviation of cell distribution vs flow rates for different cell concentrations (Re = 0.4−10.3, Wi = 0.1−3.12, El = 0.3). (d) Calculated (theoretical) maximal concentration of cells with a diameter of 13 μm, which can fit on the centerline depending on the blockage ratios β. In case of a small β, the maximum concentration is very small, because the particles are concentrated from the surrounding solution; on the other hand, at β = 1, the focusable concentration reaches a maximum. For β = 0.25, the maximum concentration of cells with a diameter of 13 μm is 28 400 000 cells per mL. (e) Cell "train" led by large cell, flow direction from left to right. (f) Cells competing for same positions on the centerline.

a flow rate of 10 μL/min, cells migrate more quickly and reach the centerline earlier than at a flow rate of 22 μL/min (Figure 2b). At higher flow rates, cells are pushed closer to the channel walls initially, resulting in delayed migration to the centerline. Accordingly, for all subsequent experiments, data were recorded 40 mm from the inlet to ensure that cells have reached their equilibrium positions.

Significantly, we observed that once a cell reaches the channel centerline, it stops rotating due to its symmetric position within the flow profile. Similar behavior has previously been reported in asymmetric situations when using a sheath flow device and viscoelastic fluids.[35] This feature unusually allows for high-resolution imaging of a specific cell multiple times during passage through the microchannel (Figure S-4a,b). Conversely, in the case of pure inertial focusing (yielding two/four equilibrium positions, Figure 1e) cells continue to rotate (Figure S-4a,c), making it difficult to image cells with high spatial resolution.

Finally, inertial flow focusing (see Supplemental Note S-3 and Figure S-5b) requires cells to travel at velocities above 0.3 m/s if efficient focusing is to be achieved. This poses significant challenges for contemporary (high sensitivity) CMOS cameras, which are characterized by relatively low frame rates. Conversely, ultrafast cameras can provide high frame rates but lack the quantum efficiency to accurately detect fluorescence signals. Accordingly, focusing of cells within a slower flow velocity regime (between 0.05 and 0.2 m/s for example) is of great importance in enabling blur-free imaging when using CMOS cameras.

Influence of Cell Concentration on Focusing Efficiency. The ability to robustly operate microfluidic systems at high cell concentrations is important in engendering high-throughput cellular analysis. To investigate the effects of concentration on focusing, experiments were performed at four different concentrations (1, 3, 6, and 12 (million cells/mL)) and over a range of flow rates (between 1 and 55 μL/min) and Reynolds numbers (between 0.4 and 10). HL60 cells (having

DOI: 10.1021/acs.analchem.7b03093
Anal. Chem. 2017, 89, 11653−11663

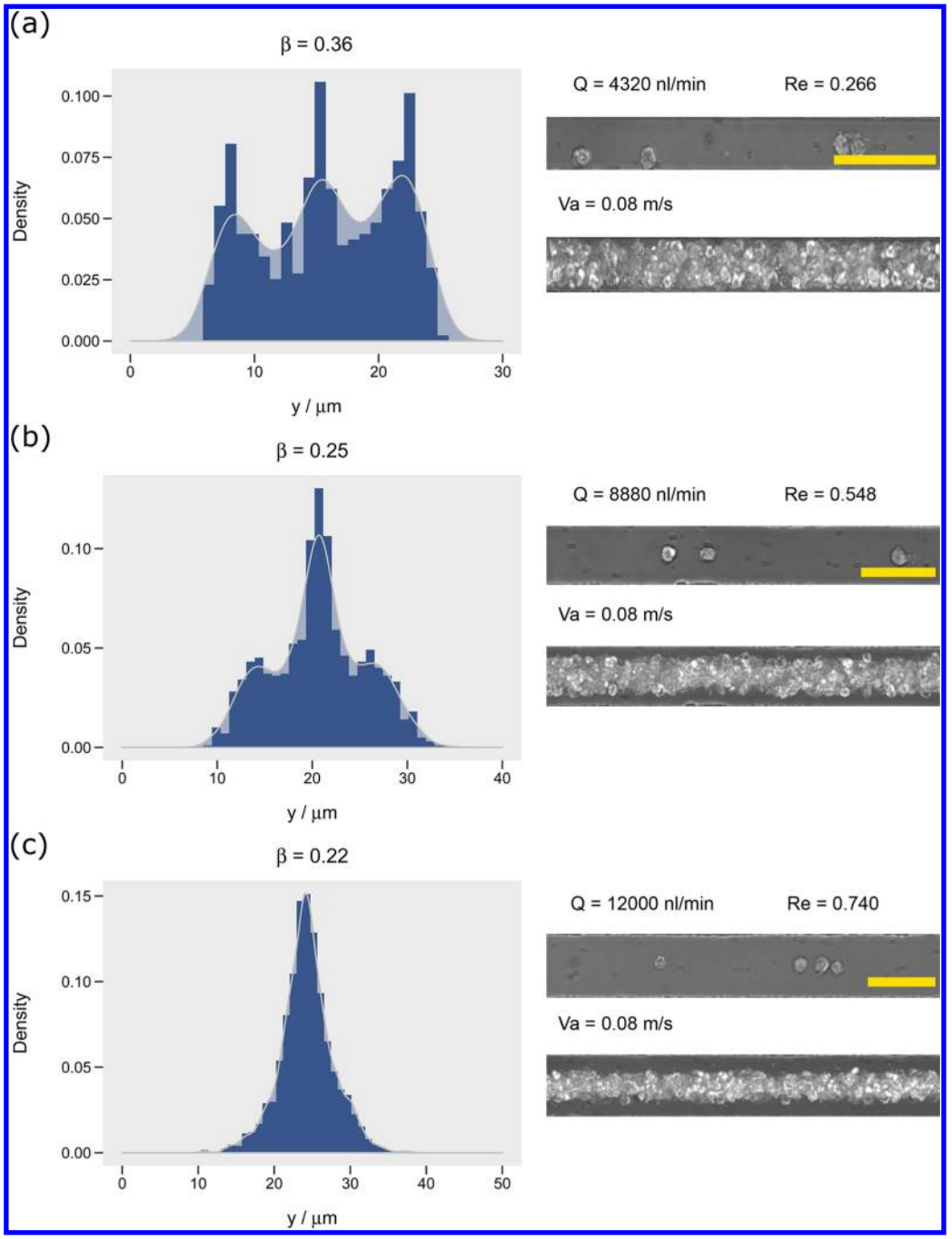

Figure 4. Distribution in y direction, single image and image stack of 3(f cells (average diameter 11 μm) immersed in a 500 ppm, 0.4 MDa PEO solution in (a) 30 × 30 μm channel (Re = 0.266, Wi = 1.6, El = 0.3), (b) 43 × 43 μm channel (Re = 0.548, Wi = 1.1, El = 0.3), and (c) 50 × 50 μm channel (Re = 0.74, Wi = 0.96, El = 0.3). Scale bars are 50 μm.

an average diameter of 13 μm, Figure S-6a) within a 53 × 53 μm cross section channel yield a blockage ratio of 0.24. This value is close to the transition between single-file focusing and focusing at multiple equilibrium positions, as will be described subsequently. Cell distribution plots for the 12 000 000 and 3 000 000 cell/mL samples (Figure 3a,b) show that radial distributions within the microchannel are broader for the higher cell concentration samples, with Figure 3c summarizing the cell focusing efficiency for all flow rates and cell concentrations. At the highest concentration (12 000 000 cells/mL) and a flow rate of 22 μL/min, cells pass along the channel as a wide band, with only 36% of the cell centers being within ±2.5 μm of the centerline. In comparison, for a concentration of 3 000 000 cells/mL, 70% of the cell centers are found within ±2.5 μm of the centerline. For 1 000 000 cells/mL, 85% can be found within this band. Below 1 000 000 cells/mL, the focusing efficiency does not increase further, because cells do not interact with each other anymore.

Two factors control the deterioration in focusing as cell concentration increases. First, as cellular concentration increases, the space per cell on the centerline of the channel decreases. For example, in the case of a 53 × 53 μm channel, the maximum concentration of cells that can be hosted on the centerline is approximately 28 000 000 cells/mL, assuming that

DOI: 10.1021/acs.analchem.7b03093
Anal. Chem. 2017, 89, 11653−11663

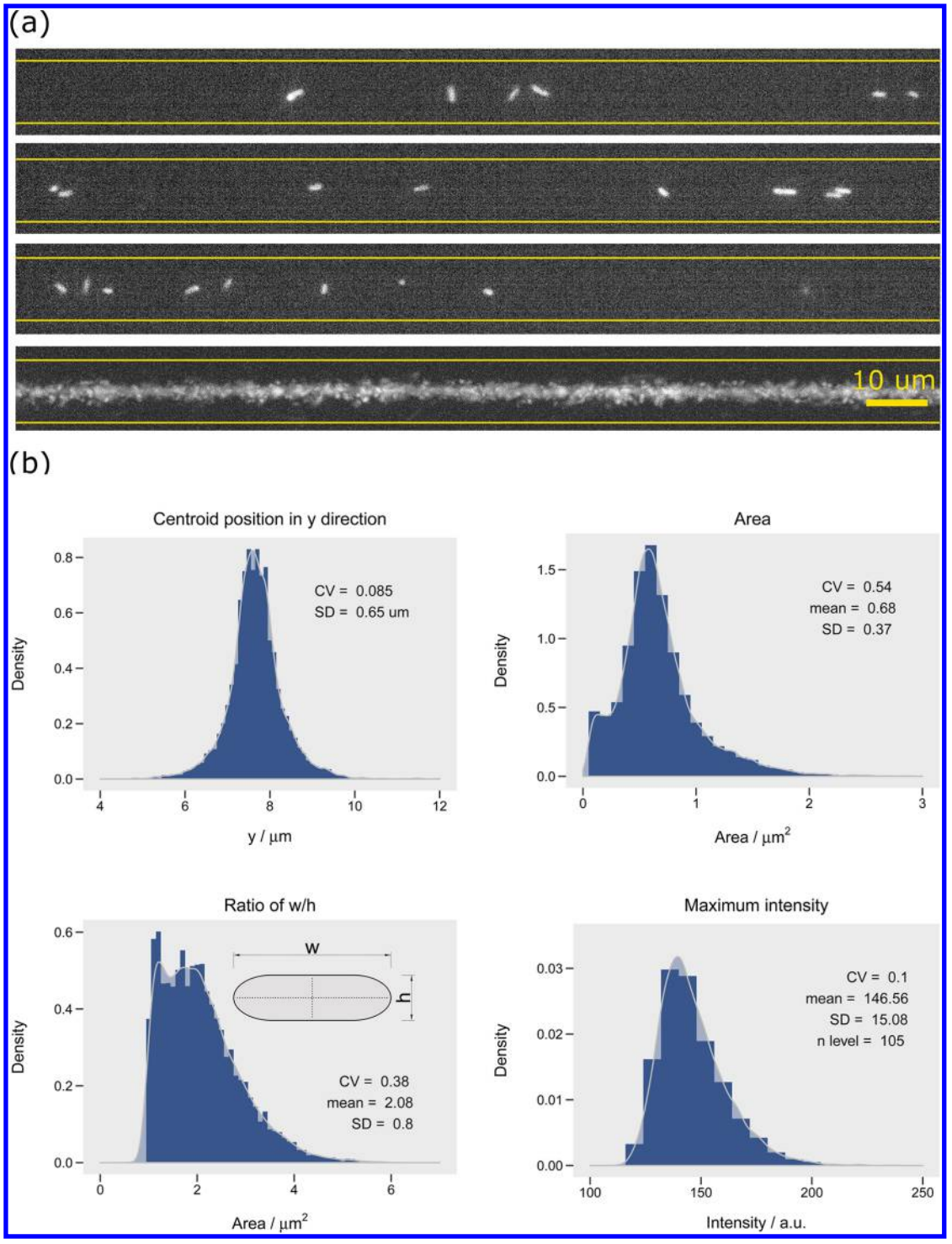

Figure 5. (a) Stroboscopic fluorescence images of fluorescently labeled *E. coli* in a 10 × 10 μm channel. The last image shows an image stack of 1000 images. Yellow lines indicate the channel wall. (b) Parameters of the bacteria, extracted from fluorescence images.

cells are side by side and touch each other. This means that as concentrations increase, cells begin to compete for the same space around the channel centerline (see theoretical curve in Figure 3f), and even if the channel length is increased (Figure 2), focusing will not improve. Second, cells within a given population will vary in size, yielding a distribution of velocities within the carrier solution, with larger cells traveling more slowly than smaller cells (Figure S-6b). Such velocity variations cause rapidly moving cells to "catch up" with slower (and larger) cells, resulting in the formation of cell chains "headed" by a large cell (for example, see Figure 3e). Such trains eventually form random cells clumps, which destroy any order.

Throughput limitations for elasto-inertial particle focusing arise from geometrical constraints (as illustrated in Figures 3f and 4) and constraints defined by the rheological properties of the carrier solution. For example, for 13 μm cells in a 53 × 53 μm channel (Figure 3f), geometrical constraints impose a concentration limit of 28 000 000 cells per mL; however, this upper limit is not achievable due to other effects, such as the formation of cell packages. Indeed, in the current experiments,

DOI: 10.1021/acs.analchem.7b03093
Anal. Chem. 2017, 89, 11653−11663

analytical throughput typically varies between 250 and 1000 cells per second, depending on cell concentration and flow rate.

It is worth noting that the concentration range between 1 000 000 and 12 000 000 cells/mL was chosen since this most closely mimics the situation in conventional flow cytometry. Indeed, the primary bottleneck to achieving higher throughput in flow cytometry remains the ability to operate at high cell concentrations, while ensuring coincident detection events are minimized. Put simply, operation at higher concentrations reduces the amount of time between adjacent events and thus increases throughput. The results shown in Figure 3c illustrate that as cell concentration increases, focusing efficiency deteriorates dramatically and the channel becomes saturated, with cells competing for the same position.

Effect of Blockage Ratio on Focusing Efficiency. Cells will typically either migrate toward the center or toward the wall of a channel under a pressure-driven flow, depending on the rheological properties of the contained fluid (shear thinning or shear thickening), the channel blockage ratio (β), and the volumetric flow rate.[19,20] In a recent study, Seo[25] showed that the blockage ratio of a viscoelastic fluid has a complex impact on particle migration within a square cross section microchannel when both elastic and inertial effects are present. The blockage ratio is defined as

$$\beta = \frac{a}{h} \tag{4}$$

where a and h are the particle diameter and the characteristic height (for a square channel $w = h$) of the microchannel, respectively.

D'Avino[33] showed that a critical radius r^* divides the space in a circular tube into two regions. Assuming that r defines the distance of the particle center point to the center of the channel, two behaviors are observed. If $r < r^*$, then the particle will move to the centerline of the channel, and if $r > r^*$, the particle is attracted to the channel wall. The value of r^* depends on the blockage ratio β, i.e. as β increases the critical radius will move toward the centerline and more cells will migrate toward the channel wall. This observation suggests that a smaller blockage ratio is preferable for achieving single-file focusing. However, as shown in Figure 3d, for high cell concentrations, tight focusing can be achieved if a higher value of β is adopted.

To more fully characterize the dependence of focusing on the blockage ratio, we investigated the cell-focusing behavior of human B-lymphoid cells (having an average diameter of 10.5 um) in a 500 ppm, 0.4 MDa PEO solution moving through channels of varying cross sections: 30 × 30, 43 × 43, and 50 × 50 μm, yielding blockage ratios of 0.36, 0.25, and 0.22 (Figure 4), respectively. The experimental flow rates were chosen to yield the same average flow velocity in each channel (~0.08 m/s), with the elasticity numbers varying between 4.8 (for the 30 × 30 μm cross section) and 1.0 (for the 50 × 50 μm cross section). In the channel with the highest blockage ratio (β = 0.36), three equilibrium positions appear in the cell center position histogram (Figure 4a), with cells tending to move closer to the wall (and away from the centerline) due to intensified shear rates (5333 s^{-1}), which in turn leads to higher compressive normal stresses in regions away from the sidewalls (5333 s^{-1}).[32] For β = 0.25 (3722 s^{-1}), the three positions contract (Figure 4b), with a further decrease in the blockage ratio to 0.22 (3200 s^{-1}) enabling single-file focusing (Figure 4c). These findings are in excellent agreement with a recent study by Yuan et al., showing a critical blockage ratio of 0.25; below this single-file focusing occurs, above this multiple equilibrium positions appear.[36] For small blockage ratios, normal stresses induced by the curvature of the velocity profile force cells to move toward the centerline, where the shear rate is vanishing.[32] Finally, the blockage ratio in combination with the cell concentration impacts focusing efficiency. At a low blockage ratio (for example, β = 0.1) cells are concentrated from the surrounding volume toward the centerline. This means that at the same cell concentration a high blockage ratio will offer more space (on the centerline) per cell compared to a low blockage ratio (as shown in Figure 3d). As the blockage ratio decreases, the maximum concentration of cells that can be focused on the centerline tends to zero, as shown in Figure 3d. Furthermore, it should be noted that the ability to focus a finite concentration of cells when the blockage ratio is large is not simply limited by geometrical constraints. First, for blockage ratios above 0.8, the microfluidic channel will become blocked prior to experiment, and second, as shown in Figure 4, blockage ratios above 0.25 will introduce multiple equilibrium positions as previously reported by Yuan et al.[36]

Bacteria Focusing for Imaging Flow Cytometry. After demonstration of precise single-file focusing of cells using the elasto-inertial approach, we extended the method to the analysis of bacterial cells (~1 μm wide and 1−5 μm long). Specifically, genetically modified bacterial cells (at a concentration of 10^6 per mL) expressing mCherrry, were immersed in the same OptiPrep-DPBS-PEO solution (500 ppm, 0.4 MDa PEO) used previously and assayed using a laser-induced stroboscopic fluorescence illumination system. Bacteria were vortexed prior to injection to prevent agglomerates, and due to the small size of bacteria, a straight microfluidic channel having cross-sectional dimensions of 10 × 10 μm and a length of 20 mm was used to maintain the same blockage ratio range as in previous experiments ($\beta \approx$ 0.1−0.2). Figure 5a shows fluorescence images of flowing bacteria and an image stack of 1000 frames. Through use of a frame rate of 550 fps, a total of 8800 bacteria were recorded within 3.6 s, yielding a throughput of >2000 bacterial cells/s. A total of 88.9% of the bacterial center points were found within ±1 μm of the centerline (96.2% within ±1.5 μm, velocity ≈ 0.025 m/s), indicating efficient and rapid single-file focusing of bacterial cells.

A unique advantage of imaging flow cytometry is the ability to extract fluorescence intensities as well as accurate size and shape information on bacteria (Figure 5 b). Furthermore, signals caused by debris or clumps can be easily discarded or ignored. Based on the processed images, the coefficient of variation (CV) of the area and anisotropy factor or aspect ratio (w/h) were calculated to be 55 and 38%, respectively. The anisotropy factor, which quantifies the length to height ratio of the bacteria is comparable to the forward scatter signal in a commercial flow cytometer. Accordingly, and for comparison, we analyzed the same bacteria sample in a conventional (nonimaging) flow cytometer (Beckman and Coulter MoFlo-Astrios, Germany), generating a CV in the forward scatter (FSC) signal of 37% (Figure S-7). The recorded images indicate that the approach can also be used to count bacterial cells at very low concentrations.

The maximum counting speed of our imaging system was estimated to be ~4000 bacterial cells s^{-1}, which provides a sensitive and rapid method for the extraction of morphological and shape-related information. Indeed, high-speed CMOS cameras can process a large number of images per second and when combined with their high sensitivity, provide a

DOI: 10.1021/acs.analchem.7b03093
Anal. Chem. 2017, 89, 11653−11663

powerful alternative to point-based flow cytometry systems. In contrast to commercial flow cytometers, where focusing relies on the use of hydrodynamic sheath flows, the elasto-inertial approach enables continuous flow-based focusing of bacteria or other submicrometer particles without dilution of the sample (caused by the sheath fluid), while consuming very small amounts of sample (~200 μL). Furthermore, if the initial concentration of bacteria or cells is small, further dilution may result in a sample with a concentration lower than achievable limits of detection. Moreover, in the case of imaging flow cytometry, when using smaller particles such as bacteria, the flow rate ratio of sheath fluid to sample needs to be high enough to achieve focusing, leading to high flow velocities, which are unfavorable if longer exposure times are desired (e.g., sensitive fluorescence imaging).

CONCLUSIONS

Herein, we have assessed and quantified the influence of different parameters (including channel geometry, cell concentration, polymer chain length, and blockage ratio) on the trajectories of cells and bacteria flowing through microchannels at high linear velocities. We have demonstrated for the first time that cells can be robustly focused either using an aged 0.1 or 0.4 MDa PEO solution at a concentration of 500 ppm (for both low and high flow rates). Significantly, for the 0.4 MDa PEO solution, efficient focusing was achieved at flow rates where pure non-Newtonian solutions already exhibit inertial focusing. This can be clearly observed in a *Wi*−*Re* plot (see Supplemental Note S-4 and Figure S-8). We also show that cell focusing in microchannels consists of primary (cells located in the centerline) and secondary (cells located close to the channel wall) populations in the highest blockage ratio channels at modest flow velocities. These can be seen as movements away from the inner wall equilibrium position and toward the center of the channel. Additionally, we have demonstrated that the blockage ratio controls not only the number of equilibrium positions but also defines the maximum concentration of cells that can be focused. The utility and simplicity of this robust focusing system is highlighted by the high-throughput imaging of fluorescently labeled *E. coli* cells and comparison to data originating from a commercial flow cytometer. Accordingly, viscoelastic focusing in microfluidic devices represents a powerful tool for the high-throughput screening and sorting of targeted rare cells such as circulating tumor cells[37] and/or bacteria[38] that display phenotypes of interest. Due to the straight channel design, throughput can be readily amplified by massive parallelization. It has also been shown that the current method can be used to focus cells without inducing bodily rotation. This feature is especially useful in morphology-based analysis of disease-infected cells and suggests the realization of an optofluidic platform for imaging and cytometric analysis in the short term.

ASSOCIATED CONTENT

Supporting Information

The Supporting Information is available free of charge on the ACS Publications website at DOI: 10.1021/acs.analchem.7b03093.

Calculations for the estimation of relaxation times of polymer solutions used for experiments; tables containing rheological properties such as Reynolds numbers, Weissenberg numbers, elasticity numbers; figure of viscosity vs shear rates for different PEO solutions; elasto-inertial focusing of polystyrene particles; images depicting different microfluidic cell focusing methods; comparison of cell focusing in Newtonian and viscoelastic fluids; forward scatter plot of bacteria from a commercial flow cytometer; cell diameter distribution and cell traveling velocimetry plots (PDF)

AUTHOR INFORMATION

Corresponding Authors

*E-mail: stavros.stavrakis@chem.ethz.ch (S.S.)
*E-mail: andrew.demello@chem.ethz.ch; Phone: +41 44 633 66 10 (A.D.)

ORCID

Andrew deMello: 0000-0003-1943-1356

Notes

The authors declare no competing financial interest.

REFERENCES

(1) Nagrath, S.; Sequist, L. V.; Maheswaran, S.; Bell, D. W.; Irimia, D.; Ulkus, L.; Smith, M. R.; Kwak, E. L.; Digumarthy, S.; Muzikansky, A.; Ryan, P.; Balis, U. J.; Tompkins, R. G.; Haber, D. A.; Toner, M. *Nature* **2007**, *450*, 1235−1239.
(2) Wu, T. H.; Chen, Y.; Park, S. Y.; Hong, J.; Teslaa, T.; Zhong, J. F.; Di Carlo, D.; Teitell, M. A.; Chiou, P. Y. Pulsed laser triggered high speed microfluidic fluorescence activated cell sorter. Proceedings of the *2012 IEEE 25th International Conference on Micro Electro Mechanical Systems (MEMS)*, Paris, France, **2012**; pp 1097−1100.10.1109/MEMSYS.2012.6170196
(3) Hur, S. C.; Mach, A. J.; Di Carlo, D. *Biomicrofluidics* **2011**, *5*, 022206.
(4) Mach, A. J.; Kim, J. H.; Arshi, A.; Hur, S. C.; Di Carlo, D. *Lab Chip* **2011**, *11*, 2827.
(5) Gossett, D. R.; Weaver, W. M.; Mach, A. J.; Hur, S. C.; Tse, H. T. K.; Lee, W.; Amini, H.; Di Carlo, D. *Anal. Bioanal. Chem.* **2010**, *397*, 3249−3267.
(6) Goda, K.; Ayazi, A.; Gossett, D. R.; Sadasivam, J.; Lonappan, C. K.; Sollier, E.; Fard, A. M.; Hur, S. C.; Adam, J.; Murray, C.; et al. *Proc. Natl. Acad. Sci. U. S. A.* **2012**, *109*, 11630−11635.
(7) Oakey, J.; Applegate, R. W., Jr; Arellano, E.; Carlo, D. D.; Graves, S. W.; Toner, M. *Anal. Chem.* **2010**, *82*, 3862−3867.
(8) Hur, S. C.; Henderson-MacLennan, N. K.; McCabe, E. R.; Di Carlo, D. *Lab Chip* **2011**, *11*, 912−920.
(9) Gossett, D. R.; Tse, H. T. K.; Lee, S. A.; Ying, Y.; Lindgren, A. G.; Yang, O. O.; Rao, J.; Clark, A. T.; Di Carlo, D. *Proc. Natl. Acad. Sci. U. S. A.* **2012**, *109*, 7630−7635.
(10) Guck, J.; Schinkinger, S.; Lincoln, B.; Wottawah, F.; Ebert, S.; Romeyke, M.; Lenz, D.; Erickson, H. M.; Ananthakrishnan, R.; Mitchell, D.; et al. *Biophys. J.* **2005**, *88*, 3689−3698.
(11) Di Carlo, D.; Edd, J. F.; Humphry, K. J.; Stone, H. A.; Toner, M. *Phys. Rev. Lett.* [Online] **2009**, *102*.10.1103/PhysRevLett.102.094503
(12) Leshansky, A.; Bransky, A.; Korin, N.; Dinnar, U. *Phys. Rev. Lett.* [Online] **2007**, *98*.10.1103/PhysRevLett.98.234501
(13) Segre, G.; Silberberg, A. *Nature* **1961**, *189*, 209−210.
(14) Martel, J. M.; Toner, M. *Annu. Rev. Biomed. Eng.* **2014**, *16*, 371−396.
(15) Di Carlo, D.; Irimia, D.; Tompkins, R. G.; Toner, M. *Proc. Natl. Acad. Sci. U. S. A.* **2007**, *104*, 18892−18897.
(16) Chung, A. J.; Gossett, D. R.; Di Carlo, D. *Small* **2013**, *9*, 685−690.
(17) Karnis, A.; Mason, S. *Trans. Soc. Rheol.* **1966**, *10*, 571−592.
(18) Ho, B.; Leal, L. *J. Fluid Mech.* **1976**, *76*, 783−799.
(19) Morris, J. F.; Boulay, F. *J. Rheol.* **1999**, *43*, 1213−1237.
(20) Romeo, G.; D'Avino, G.; Greco, F.; Netti, P. A.; Maffettone, P. L. *Lab Chip* **2013**, *13*, 2802−2807.

DOI: 10.1021/acs.analchem.7b03093
Anal. Chem. 2017, 89, 11653−11663

(21) Kang, K.; Lee, S. S.; Hyun, K.; Lee, S. J.; Kim, J. M. *Nat. Commun.* [Online] **2013**, *4*.10.1038/ncomms3567
(22) Yang, S.; Kim, J. Y.; Lee, S. J.; Lee, S. S.; Kim, J. M. *Lab Chip* **2011**, *11*, 266−273.
(23) Kim, B.; Kim, J. M. *Biomicrofluidics* **2016**, *10*, 024111.
(24) Lim, E. J.; Ober, T. J.; Edd, J. F.; Desai, S. P.; Neal, D.; Bong, K. W.; Doyle, P. S.; McKinley, G. H.; Toner, M. *Nat. Commun.* [Online] **2014**, *5*.10.1038/ncomms5120
(25) Seo, K. W.; Kang, Y. J.; Lee, S. J. *Phys. Fluids* **2014**, *26*, 063301.
(26) Ciftlik, A. T.; Ettori, M.; Gijs, M. A. *Small* **2013**, *9*, 2764−2773.
(27) Kalashnikov, V. J. *J. Rheol.* **1994**, *38*, 1385−1403.
(28) Han, Y.; Gu, Y.; Zhang, A. C.; Lo, Y.-H. *Lab Chip* **2016**, *16*, 4639−4647.
(29) Lau, A. K.; Shum, H. C.; Wong, K. K.; Tsia, K. K. *Lab Chip* **2016**, *16*, 1743−1756.
(30) Fu, A. Y.; Chou, H.-P.; Spence, C.; Arnold, F. H.; Quake, S. R. *Anal. Chem.* **2002**, *74*, 2451−2457.
(31) Takahashi, K.; Hattori, A.; Suzuki, I.; Ichiki, T.; Yasuda, K. *J. Nanobiotechnol.* **2004**, *2*, 5.
(32) Huang, P.; Feng, J.; Hu, H. H.; Joseph, D. D. *J. Fluid Mech.* **1997**, *343*, 73−94.
(33) D'Avino, G.; Romeo, G.; Villone, M. M.; Greco, F.; Netti, P. A.; Maffettone, P. L. *Lab Chip* **2012**, *12*, 1638−1645.
(34) Villone, M.; D'Avino, G.; Hulsen, M.; Greco, F.; Maffettone, P. *J. Non-Newtonian Fluid Mech.* **2011**, *166*, 1396−1405.
(35) Lu, X.; Xuan, X. *Anal. Chem.* **2015**, *87*, 11523−11530.
(36) Yuan, D.; Tan, S. H.; Zhao, Q.; Yan, S.; Sluyter, R.; Nguyen, N.; Zhang, J.; Li, W. *RSC Adv.* **2017**, *7*, 3461−3469.
(37) Nagrath, S.; Sequist, L. V.; Maheswaran, S.; Bell, D. W.; Irimia, D.; Ulkus, L.; Smith, M. R.; Kwak, E. L.; Digumarthy, S.; Muzikansky, A.; et al. *Nature* **2007**, *450*, 1235−1239.
(38) Choi, J.; Kang, M.; Jung, J. H. *Sci. Rep.* [Online] **2015**, *5*.10.1038/srep15983

DOI: 10.1021/acs.analchem.7b03093
Anal. Chem. 2017, 89, 11653−11663